Bacteria-Inspired Magnetic Polymer Composite Microrobots

Kathrin E. Peyer[1], Erdem C. Siringil[1], Li Zhang[2], Marcel Suter[3], and Bradley J. Nelson[1]

[1]Institute of Robotics and Intelligent Systems, ETH Zurich, Switzerland
bnelson@ethz.ch
[2]Department of Mechanical and Automation Engineering, The Chinese University of Hong Kong
[3]Micro and Nanosystems, ETH Zurich, Switzerland

Abstract. Remote-controlled swimming microrobots are promising tools for future biomedical applications. Magnetically actuated helical microrobots that mimic the propulsion mechanism of *E. coli* bacteria are one example, and presented here is a novel method to fabricate such microrobots. They consist of a polymer-nanoparticle composite, which is patterned using a direct laser writing tool. The iron-oxide nanoparticles respond to the externally applied low-strength rotating magnetic field, which is used for the actuation of the microrobots. It is shown that a helical filament can be rotated around its axis without the addition of a body part and without structuring the magnetization direction of the composite. The influence of the helicity angle on the swim behavior of the microrobots is examined and experimental results show that a small helicity angle of 20 degrees is preferred for weakly magnetized microstructures.

Keywords: Bio-inspired microrobots, swimming microrobots, magnetic actuation, magnetic polymer composite.

1 Introduction

Remote controlled swimming microrobots are an emerging field of research as they are promising tools in medical applications, such as targeted drug delivery [1], or for *in vitro* experimentation, such as single cell manipulation and characterization [2]. The design challenges revolve around the fact that these robots are only a few micrometers in size. Firstly, they navigate at a low Reynolds (Re) number regime, which dictates the type of suitable locomotion method that can be employed. Secondly, the question of power supply has to be solved. Thirdly, the microrobots should be non-toxic and be able to interact safely with living cells. And finally, fabrication methods have to be found to make devices that fulfill the previous three criteria.

There are a number of recently published micro-devices that have successfully addressed some of these design challenges, although not necessarily solving all

N.F. Lepora et al. (Eds.): Living Machines 2013, LNAI 8064, pp. 216–227, 2013.

of them at once. For example, possible means of power supply include the use of temporal and spatially varying magnetic fields or chemical gradients [3],[4]. Chemically fueled devices have been used for *in vitro* experiments and can reach high velocities of several body lengths per second. The difficulty is to establish the chemical gradients in the experimental environment, which is why they cannot easily be implemented *in vivo* or when handling sensitive cells. Low-strength and low-frequency magnetic fields, on the other hand, can be employed *in vitro* as well as *in vivo*. The magnetic field strengths necessary for actuating microrobots lie in order of a few milli Tesla, which is much lower than the field strength of a magnetic resonance imaging (MRI) system (reaching up to 3 Tesla).

Due to their size, microrobots swim at a low Reynolds (Re) number, which is a measure for inertial versus viscous forces in a liquid. Baceria, such as *E. coli*, move in this viscous environment by rotating one or several helical filaments with a molecular rotary motor [10]. The helical filament transforms rotational into translatory motion, similar to a corkscrew (see Fig. 1). Microrobots employing this bio-mimicking helical locomotion method have been published previously, such as the first artificial bacterial flagella (ABFs) by Bell [5], the propellers by Ghosh [6], and more recently the polymer ABFs by Tottori [7]. All these devices are actuated by uniform rotating magnetic fields.

The first two reported prototypes were manufactured by batch fabrication methods that limit the type of shapes that can be achieved [5], [6]. Tottori employed a direct laser writing (DLW) method, which allows the fabrication of almost arbitrarily-shaped structures from a variety of photosensitive polymers [7]. The magnetic material necessary for the robot actuation has to be deposited in a second fabrication step. Recently, Suter et al. developed a magnetic polymer composite (MPC) with superparamagnetic properties [8]. This MPC can be patterned by the same DLW tool. The advantage of using MPC is that the magnetic material is already incorporated into the polymer. Furthermore, the material has been shown to be non-cytotoxic [9].

This paper presents the characterization and modeling of the swim behavior of MPC helical microrobots fabricated using the DLW method and actuated by

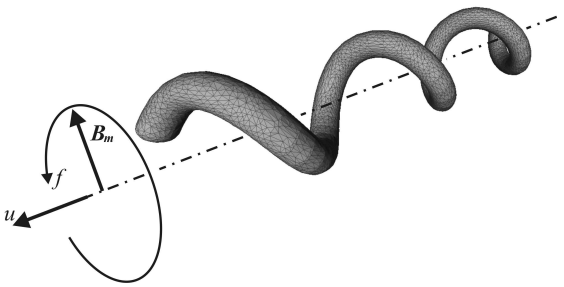

Fig. 1. Schematic of a magnetic helical microrobot. A magnetic field $\boldsymbol{B_m}$ is rotated around the helical axis at a frequency f. The magnetic torque rotates the robot and its helical shape transforms the rotation into a linear velocity u.

uniform rotating magnetic fields. Several prototypes were fabricated and their swim performance tested. It is shown that the helicity angle plays an important role in how the structures magnetize, and this determines the success or failure at achieving corkscrew-type swimming motion.

2 Magnetic Helical Microrobots

2.1 Helical Propulsion

Helical propulsion at low Re numbers has been studied for several decades by biologists interested in the locomotion of microorganisms [11],[12], and recently with respect to microrobots [13]. The linear relationship between the drag forces $\boldsymbol{F_d}$ and torques $\boldsymbol{T_d}$ and the object's velocity $\boldsymbol{U}$ and rotational speed $\boldsymbol{\Omega}$ can be represented by a 6×6 resistance matrix.

$$\begin{pmatrix} \boldsymbol{F_d} \\ \boldsymbol{T_d} \end{pmatrix} = - \begin{pmatrix} A & B \\ B^T & C \end{pmatrix} \begin{pmatrix} \boldsymbol{U} \\ \boldsymbol{\Omega} \end{pmatrix} \tag{1}$$

A, B, and C are 3x3 matrices and are functions of the object's geometry and fluid viscosity only. A number of methods have been employed to model low Re flows and resistance matrices, such as the method of fundamental solutions, the boundary element method, or the method of regularized stokeslets, which is the method chosen in this paper (see Section 3.3). The resistance matrix of a helix contains non-zero elements in B, which model the coupling between the rotational and translatory motion.

2.2 Magnetic Actuation

Using helical filaments brings advantages when considering the magnetic actuation of microrobots. Abbott *et al.* investigated the scaling of magnetically actuated swimming microrobots and compared magnetic force-driven with magnetic torque-driven devices [14]. It was shown that torque-driven devices scale favorably over force-driven devices as the size of the device decreases to the microscale. This supports the use of helical propulsion for magnetic microrobots as it only relies on the application of a torque to rotate the device rather than on a force to pull it.

A magnetized body aligns itself with the direction of an external magnetic field, in the same manner as a compass needle aligns with the earth's magnetic field lines. This magnetic torque can be used to rotate microstructures in a controlled manner. The magnetic torque $\boldsymbol{T_m}$ acting on a body with volume V is

$$\boldsymbol{T_m} = V \cdot \boldsymbol{M} \times \boldsymbol{B_m} \tag{2}$$

where $\boldsymbol{M}$ is the magnetization and $\boldsymbol{B_m}$ the external magnetic field. The magnetic field vector $\boldsymbol{B_m}$ is rotated at a frequency f. The magnetization $\boldsymbol{M}$ is constant for a permanently magnetized body or it is a function of the applied field and the

body geometry for soft-magnetic materials. For simple shapes, such as bodies of revolution, the magnetization can be modeled analytically, but no such solutions exist for a helical body.

In order to actuate the ABF a torque has to be applied in the direction of the helical axis. This can only be achieved if the magnetization is not parallel to the helical axis and is optimal for a magnetization perpendicular to the helical axis. Many previous publications used special means to influence the magnetization of their helical microrobots, such as adding a magnetic head plate [5], permanently magnetizing the structure [6], or aligning the nanoparticles [16]. It is, however, possible to generate an actuation torque even for a helix without aligned magnetization [7]. The structures presented here do not have a pre-aligned magnetization and their response to the magnetic actuation will be discussed in Section 5.

2.3 Microrobot Propulsion Model

To model the behavior of the microrobot, the magnetic and fluid mechanical model of Eq. (1) and (2), respectively, are combined. The equation can be simplified by considering only the rotation around and the translation along the helical axis. This results in a simple 2×2 resistant matrix with scalar entries a, b and c. Furthermore, the external force is assumed to be zero because the helix moves in a horizontal, unobstructed plane, and without the application of magnetic gradient forces.

$$\begin{pmatrix} 0 \\ T_m \end{pmatrix} = \begin{pmatrix} a & b \\ b & c \end{pmatrix} \begin{pmatrix} u \\ 2\pi f \end{pmatrix} \tag{3}$$

At any given low rotational frequency $f < f_{stepout}$ of the magnetic field $\boldsymbol{B_m}$ (see Fig. 1), the magnetic torque T_m is such that it counterbalances the fluidic drag $T_d = -(bu + c2\pi f)$, and the velocity is linearly related to f:

$$u = -\frac{b}{a} 2\pi f = p_{eff} \cdot f \tag{4}$$

The 'effective pitch' $p_{eff} = -2\pi b/a$ describes how far the helix advances forward per rotation. Unlike a corkscrew in solid material, the helix slips when moving in the fluid and p_{eff} is, therefore, only a small fraction of the actual, i.e. geometric, pitch length of the helix.

If the frequency is increased above the step-out frequency $f_{stepout}$, the fluidic drag exceeds the maximal available magnetic torque $T_{m,max}$. The robot falls out of sync with the magnetic field and starts to oscillate backwards and forwards around its axis, which leads to a decrease in velocity. It is therefore desirable to have microrobots with large step-out frequencies.

3 Experimental Methods

3.1 Fabrication

The magnetic polymer composite (MPC) was developed by Suter and consists of SU-8 50 and a magnetite nanoparticle (Fe_3O_4) suspension. Details on the process for creating a uniform suspension of the nanoparticles in the viscous SU-8 can be found in this publication [8]. In order to create 3D helical structures, a DLW tool by Nanoscribe Inc. was used. The fabrication process is based on the two-photon polymerization of the photosensitive SU-8 at the focal point of the laser. A piezoelectric stage moves the substrate along the predefined helical trajectory. The nanoparticles introduced in the polymer scatter and absorb the laser beam, and inhibit the polymerization reaction if the concentration is too large [9]. The line resolution is on the order of a few hundred nanometers. Composite structures were written with 4 vol.% and 2 vol.% nanopatricle fill factors, but reproducible results were only accomplished with the 2 vol.% composite. Figure 2 shows SEM images of a 2 vol.% and 4 vol.% 3-turn helix. In order to increase stability, several lines were written to achieve a filament thickness of 1.8μm. Helices with helicity angles of $\Psi = (20, 30, 40, 50)$ degrees were fabricated from the 2 vol.% MPC, while the helix radius was kept constant at $R = 2.25$μm.

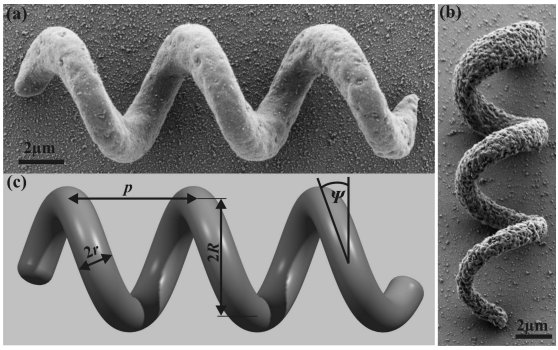

Fig. 2. Helical microrobot prototypes. (a) SEM image of an MPC microrobot with a nanoparticle fill factor of 2 vol.%. (b) SEM image of an MPC microrobot with a nanoparticle fill factor of 4 vol.%. Due to the increased quantity of nanoparticles the 4 vol.% MPC does not get polymerized uniformly. The polymerization depends on the polymer layer depth, which results in a different filament thickness along the structure. (c) Corresponding CAD model. The main design parameters are the helix radius R, the filament radius r, the helicity angle Ψ, and the pitch p.

3.2 Experimental Setup

The swim tests were conducted in deionized water in a small tank at the center of three orthogonally placed Helmholtz coil pairs. Helmholtz coils achieve an almost uniform magnetic field in their center. Hence, the magnetic forces acting

on the microrobot are negligible. The setup can generate rotating magnetic fields with strengths up to $|\boldsymbol{B_m}| = 10\text{mT}$. All the experiments are performed under a microscope and the images recorded at 30 fps by a camera with a resolution of 640×480 pixels. More details of the experimental setup can be found in previous publications [17].

3.3 Numerical Model

Resistance Matrix. In order to solve Eq. 3, the entries of the resistance matrix have to be known. As mentioned previously, they are only a function of the geometrical parameters and the viscosity of the fluid. There are analytical solutions for a slender helix [13]. The MPC microrobots, however, do not fulfill the slenderness criteria and numerical methods have to be employed. It is possible to superimpose singularity solutions due to linearity of the Stokes equation that governs low Re fluid mechanics. The problem with the superposition of fundamental solutions, of which the most famous is called the stokeslet, is that the solutions are singular at their source point. Cortez adapted this method by introducing a spreading function to regularize the stokeslet, and other fundamental solutions, and thereby removing the singularity at the source point [18]. The resistance of an object can be approximated by a distribution of regularized stokeslets over the surface of the body. The surface of the microrobot was discretized (see Fig. 1) and Cortez's algorithm implemented in C++ to calculate the entries of the resistance matrix.

Magnetization. In order to capture the basic actuation behavior for an optimal microrobot, soft-magnetic properties were assigned to the robot with the easy magnetization axis being perpendicular to the helical axis. This does not represent the non-ideal magnetization direction in the different robot designs, but is sufficient to model the step-out behavior as a function of different externally applied magnetic field strengths. The magnetization model as well as the motion model Eq. 3 were implemented in MATLAB®.

4 Experimental Results

4.1 Frequency-Dependent Swim Behavior

Microrobots with helicity angles of $\Psi = (20, 30, 40, 50)$ degrees were tested and their swim behavior recorded. It has previously been reported that magnetically actuated microswimmers show a dynamic behavior where they exhibit a wobbling around the helical axis with a frequency-dependent precession angle [15]. It was shown that motion changes from tumbling, i.e. a precession angle of 90 degrees, to corkscrew-type motion around the helical axis when the actuation frequency is increased. Fig. 3 shows video excerpts from the swim tests of the different prototypes. Fig. 3 (a) and (b) show the same microrobot ($\Psi = 20$ degree) at different frequencies and the change in wobbling angle β is apparent.

The other microrobots ($\Psi = 30, 40, 50$ degree) all rotate with a precession angle of 90 degrees. Increasing the actuation frequency did not result in a decreasing wobbling angle. These designs were abandoned and the following experiments were conducted only with 20-degree prototypes.

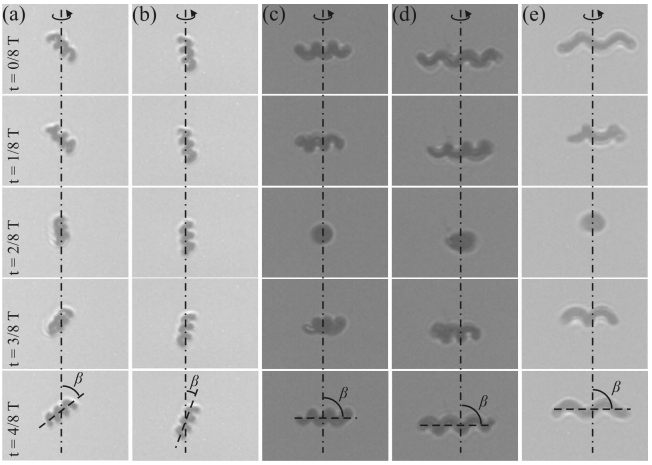

Fig. 3. Tumbling motion of robot prototypes with helicity angles of 20 (a) and (b), 30 (c), 40 (d), and 50 (e) degrees. Each image sequence (top to bottom) shows a half turn; T denotes the period time $T = 1/f$. The dash-dotted line indicates the axis of rotation. (a) and (b) show the same 20-degree helicity angle microrobot at two different frequencies. This prototype exhibits typical frequency-dependent wobbling, which decreases with increasing frequency; i.e., the precession angle decreases from (a) approximately 45 degrees at a $f = 0.5$Hz to (b) approximately 20 degrees at $f = 1$Hz. (c) - (e) shows microrobots with a helicity angles of 30, 40 and 50 degrees, respectively. They tumble at all input frequencies without reorienting to a screw-type motion.

4.2 Influence of Magnetic Actuation

The wobbling angles for several 20-degree microrobot prototype were measured for different frequencies and different magnetic field strengths. As expected, the wobbling decreased with frequency but increased with magnetic field strength (see Fig. 4). With small wobbling angles, the microrobots achieved a corkscrew-type motion, where they were propelled forward. Fig. 5 shows the successful propulsion of two prototypes. They moved simultaneously because they received the same magnetic input. They were steered by changing the direction of the rotating magnetic field.

Fig. 6 shows how the magnetic field strength influences the velocity of the swimmer. The velocity increased with frequency until the step-out frequency $f_{stepout}$ was reached, where the velocity suddenly dropped. The step-out frequency increased with the magnetic field strength. Additionally, a shift of the linear frequency-velocity region to the right was observed when the field strength

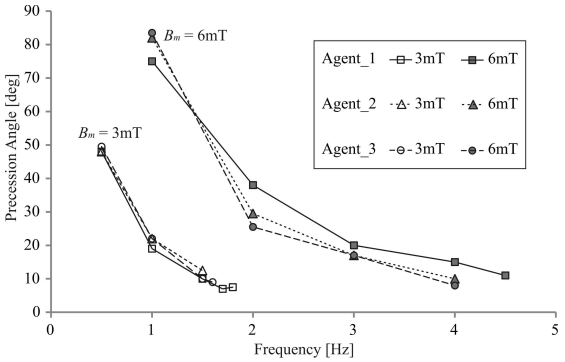

Fig. 4. The precession angle at different actuation frequencies and magnetic field strengths. The precession angle is measured between the axis of the helix and the axis of rotation (see Fig. 3).

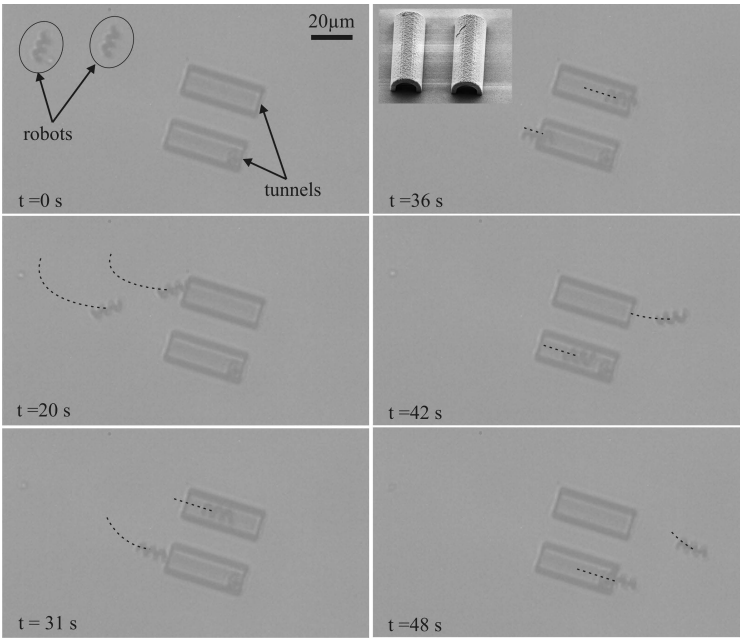

Fig. 5. Video sequence showing the simultaneous steering of two microrobots ($\Psi = 20$ degree). They are steered through two adjacent tunnels on the substrate. The inset shows an SEM image of the two tunnels.

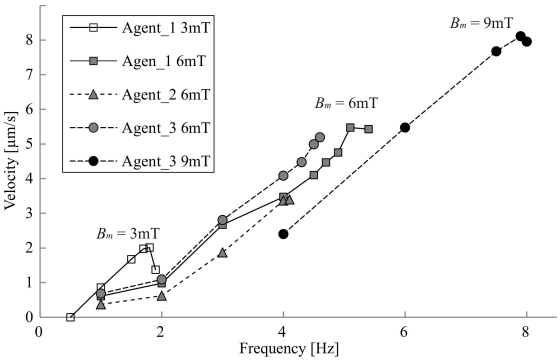

Fig. 6. Frequency-velocity plot at magnetic field strengths $|\boldsymbol{B_m}| = 3$, 6, and 9 mT.

was increased. Finally, Fig. 7 contains the result from a 4vol.% MPC microrobot in comparison to a 2vol.% prototype. The simulation results in Fig. 7 and all the experimental results will be discussed in detail in the next section.

5 Discussion

5.1 Frequency-Dependent Swim Behavior

There have been a number of previous publications that reported the frequency-dependent swim behavior of magnetic helical microrobots [15],[7]. It was, therefore, expected that similar results with the MPC structures presented in this paper would be seen. Instead, the helices with the helicity angles larger than 20 degrees did not stabilize to a corkscrew motion even as the frequency was increased. It appears that the direction and magnitude of the microrobot's magnetization play an important role. Fig. 8 shows a schematic representation of a typical experimental result. At low frequencies, there is a large precession angle, which minimizes the forward motion. Only when the precession angle decreases does the linear frequency-velocity behavior appear. The change from tumbling to a corkscrew-type motion occurs at the stabilization frequency f_{stable}, indicated by the vertical dash-dot line in Fig. 8. At high frequencies the step-out frequency $f_{stepout}$, indicated by the vertical dotted line, is reached and the microrobot loses speed again. For $f_{stable} < f_{stepout}$, there exists a linear velocity region where screw-type locomotion occurs.

The wobbling is increased when the magnetization of the microrobot is not perfectly perpendicular to the helical axis. The results published by Tottori indicate that magnetization of helical structures is strongly influenced by the helicity angle [7]. The further away the magnetization vector is from the desired 90 degrees to the helical axis, the higher the stabilization frequency f_{stable}. If f_{stable} becomes too large, i.e. $f_{stable} > f_{stepout}$, the corkscrew motion disappears and the microrobot goes from tumbling directly into step-out behavior, which is

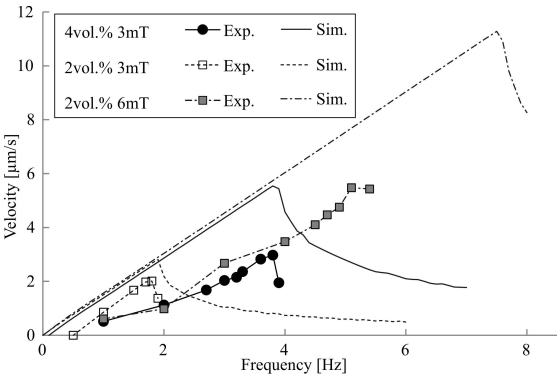

Fig. 7. Comparison of 2vol.% and 4vol.% MPC structures with experimental and simulation results. At $|\boldsymbol{B_m}| = 3$mT the step-out frequency of the 4vol.% MPC is approximately double to the 2vol.% MPC. Increasing the external magnetic field has a larger impact than increasing the amount of magnetic material.

the behavior observed with the 30-, 40-, and 50-degree helicity angle structures in Fig. 3. The helicity angle is not the only factor that influences f_{stable}. For example, an overall slender microrobot design can decrease f_{stable} as well.

5.2 Influence of Magnetic Actuation

The magnetic field strength influences the tumbling behavior by increasing the stabilization frequency f_{stable} (from approximately 2Hz to around 4Hz in Fig. 4). A strong magnetic field also increases $f_{stepout}$ and therefore still allows for a screw-type swimming region. Fig. 6 shows the resulting forward velocity gained by increasing the magnetic field strength. The linear corkscrew region is shifted to higher frequencies. It is important to note that the magnetic field does not influence the frequency-velocity slope, i.e. the 'effective pitch' p_{eff}, in the linear corkscrew region. The same holds true for increasing the magnetization of the microrobot. Fig. 7 shows the 2vol.% MPC microrobot in comparison to the 4vol.% MPC. The figure also contains the simulation data of the velocity and step-out frequency from Eq. 3. The simulation assumes a magnetization perpendicular to the helical axis, which is why it predicts a $f_{stable} = 0$ unlike the experimental data. The magnetic material properties of the simulation were tuned to achieve a step-out frequency of approximately 2Hz for the 2vol.% MPC at 3mT.

The simulation predicts that doubling the amount of magnetic nano-particles in the polymer results in approximately double the step-out frequency, which corresponds well to the experimental results. Doubling the applied magnetic field to 6mT should quadruple the step-out frequency. This can also be seen from examining Eq. 2. The maximum magnetic torque is a function of the applied field and the magnetization of the microrobot. For soft-magnetic or super-paramagnetic

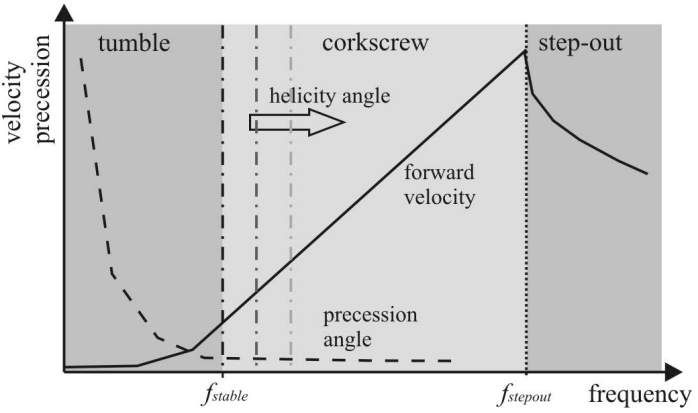

Fig. 8. Schematic representation of magnetic helical swimmers. At low frequency tumbling occurs. Increasing the frequency beyond f_{stable} stabilizes the motion into a screw-type motion. At the limit of the available magnetic torque, the step-out frequency $f_{stepout}$ is reached. The helicity angle Ψ increases f_{stable}, which eventually leads to $f_{stable} > f_{stepout}$, where no corkscrew motion appears as observed in Fig. 3 (c)-(e).

materials, the magnetization itself is a function of the applied field. For small magnetic field strengths this relationship is approximately linear, which results in a quadrupling of $T_{m,max}$, and therefore $f_{stepout}$, when $|\boldsymbol{B_m}|$ is doubled. In the experiments, the step-out frequency for $|\boldsymbol{B_m}| = 6\text{mT}$ is, however, smaller than that. This may be explained by the different magnetic saturation behavior of nanoparticle composited compared to bulk material.

6 Conclusion

Bacteria-inspired swimming microrobots can be actuated and guided remotely via low-strength rotating magnetic fields. Helical swimming microbots made of a nanoparticle-polymer composite have been fabricated and investigated. One of their main advantages is the straightforward fabrication method by direct laser writing and their non-cytotoxicity. It was shown that the helicity angle plays an important role for the swimming behavior. Designs with helicity angles of 30 degrees or larger were not able to achieve corkscrew motion. The 20-degree prototypes, on the other hand, stabilized from tumbling to a screw-type motion, and their maneuverability was demonstrated Fig. 5.

Acknowledgments. The authors thank the financial support from the Swiss National Science Foundation, contract No. 200021_130069.

References

1. Nelson, B.J., Kaliakatsos, I.K., Abbott, J.J.: Microrobots for Minimally Invasive Medicine. Ann. Rev. Biomed. Eng. 28, 55–85 (2010)
2. Zhang, L., Peyer, K.E., Nelson, B.J.: Artificial Bacterial Flagella for Micromanipulation. Lab Chip 10, 2203–2215 (2010)
3. Peyer, K.E., Zhang, L., Nelson, B.J.: Bio-Inspired Magnetic Swimming Microrobots for Biomedical Applications. Nanoscale 5, 1259–1272 (2013)
4. Sanchez, S., Solovev, A.A., Schulze, S., Schmidt, O.G.: Controlled Manipulation of Multiple Cells Using Catalytic Microbots. Chem. Commun. 47, 698–700 (2011)
5. Bell, D.J., Leutenegger, S., Hammer, K.M., Dong, L.X., Nelson, B.J.: Flagella-like Propulsion for Microrobots Using a Magnetic Nanocoil and Rotating Electromagnetic Field. In: Proc. IEEE Int. Conf. Robotics and Automation, pp. 1128–1133 (2007)
6. Ghosh, A., Fischer, P.: Controlled Propulsion of Artificial Magnetic Nanostructured Propellers. Nano Lett. 9, 2243–2245 (2009)
7. Tottori, S., Zhang, L., Qiu, F., Krawczyk, K., Franco-Obregón, A., Nelson, B.J.: Magnetic Helical Micromachines: Fabrication, Controlled Swimming, and Cargo Transport. Adv. Mater. 24, 811–816 (2012)
8. Suter, M., Ergeneman, O., Zürcher, J., Moitzi, C., Pané, S., Rudin, T., Pratsinis, S.E., Nelson, B.J., Hierold, C.: A Photocurable Superparamagnetic Nanocomposite: Material Characterization and Fabrication of Microstructures. Sens. Act. 156, 433–443 (2011)
9. Suter M., Zhang, L., Siringil, E. C., Peters, C., Luehmann, T., Ergeneman, O., Peyer, K. E., Nelson, B. J., Hierold, C.: Superparamagnetic Microrobots: Fabrication by Two-Photon Polymerization and Biocompatibility (submitted for publication)
10. Berg, H.C., Anderson, R.A.: Bacteria Swim by Rotating Their Flagellar Filaments. Nature 245, 380–382 (1973)
11. Taylor, G.: Analysis of the Swimming of Microscopic Organisms. Proc. Nat. Acad. Sci. 209, 447–461 (1951)
12. Lighthill, J.: Flagellar Hydrodynamics. SIAM Rev. 18, 161–230 (1976)
13. Mahoney, A.W., Sarrazin, J.C., Bamberg, E., Abbott, J.J.: Velocity Control with Gravity Compensation for Magnetic Helical Microswimmers. Adv. Robot. 25, 1007–1028 (2011)
14. Abbott, J.J., Peyer, K.E., Lagomarsino, M.C., Zhang, L., Dong, L., Kaliakatsos, I.K., Nelson, B.J.: How Should Microrobots Swim? Int. J. Robot. Res. 28, 1434–1447 (2009)
15. Peyer, K.E., Zhang, L., Kratochvil, B.E., Nelson, B.J.: Non-ideal Swimming of Artificial Bacterial Flagella Near a Surface. In: Proc. IEEE Int. Conf. Robotics and Automation, pp. 96–101 (2010)
16. Peters, C., Ergeneman, O., Nelson, B.J., Hierold, C.: Superparamagnetic Swimming Microrobots with Adjusted Magnetic Anisotropy. In: Proc. IEEE Int. Conf. Micro Electro Mechanical Systems, pp. 564–567 (2013)
17. Peyer, K.E., Mahoney, A.W., Zhang, L., Abbott, J.J., Nelson, B.J.: Bacteria-Inspired Microrobots. In: Kim, M., Steager, E., Julius, A. (eds.) Microbiorobotics, pp. 165–199. Elsevier (2012)
18. Cortez, R., Fauci, L., Medovikov, A.: The Method of Regularized Stokeslets in Three Dimensions: Analysis, Validation, and Application to Helical Swimming. Phys. Fluid. 17, 031504 (2005)